Electrocatalysis (2023) 14:325–331
https://doi.org/10.1007/s12678-022-00802-x

RESEARCH

Density Functional Calculations of the Sequential Adsorption of Hydrogen on Single Atom and Small Clusters of Pd and Pt Supported on Au(111)

Joshua Meléndez-Rivera[1] · **Juan A. Santana**[1]

Accepted: 4 December 2022 / Published online: 9 December 2022

Abstract
We have used density functional theory calculations to study the sequential adsorption of hydrogen on Pd and Pt atomic site catalysts such as single-atom alloy catalysts (SAAC), single-atom catalysts (SAC), and single cluster catalysts (SCC) on Au(111). The results show that Pd systems tend to have near-zero free energy of hydrogen adsorption ($\Delta G_{H_{ads}} \approx 0$) under various coverage conditions of adsorbed hydrogen. In the case of Pt systems, $\Delta G_{H_{ads}} \approx 0$ only at high coverage conditions of adsorbed hydrogen. Such differences come from the preference of hydrogen for high-coordination and low-coordination sites on Pd and Pt, respectively. The low coordination of hydrogen results in multiple adsorption sites with $\Delta G_{H_{ads}} \approx 0$ in SCC of Pt/Au. These results can help to understand the different catalytic properties of Pd/Au and Pt/Au.

Keywords Electrocatalysis · Mixed metal · Nanoelectrodes · Hydrogen evolution · Hydrogen spillover

Introduction

Site coordination plays a significant role in catalysis [1–5]. In the case of metal-supported metal electrocatalysts, the experimental techniques for preparing well-defined systems and the instrumentations to identify differences in coordination have become available only recently [6, 7]. The new methods and instrumentations have provided invaluable details on the role of site coordination in the catalysis of metal-supported metal electrocatalysts. The step-like sites in Pt/Au(111) were shown to contribute more to the overall catalytic activity in hydrogen evolution reaction (HER) than either the Pt or Au terrace sites [8]. In another study, the electrochemical scanning tunneling microscope (n-ECSTM) method was used to show that the catalytic activity for HER is different for Pd and Pt nanoislands on Au(111) [9]. It was found that the catalytic activity is maximal at the Pd/Au boundary while relatively uniformly across the Pt/Au boundary and the inner region of the Pt nanoislands [9]. These differences between Pt/Au and Pd/Au were rationalized initially in terms of the interplay between ligand and strain effects. It was postulated that Au tensile strain effects dominate in the case of Pt/Au, but both ligand and strain effects played a role in Pd/Au [9].

However, we used density functional theory (DFT) calculations to show that Au tensile strain is 50% larger in Pd/Au than in Pt/Au [10]. We postulated that instead, the catalytic activity is different for Pd/Au and Pt/Au nanoislands because, for Pd, there are sites with the near-zero free energy of hydrogen adsorption ($\Delta G_{H_{ads}} \approx 0$) only at the Pd/Au boundary, while such sites are at the Pt/Au boundary and inner region of the Pt nanoislands [11]. Such differences come from the preference of hydrogen for low-coordination and high-coordination sites on Pt and Pd, respectively, which can be traced to relativistic contraction and stabilization of the valence s-orbital in Pt [12, 13]. These computational results reveal multiple sites with a free energy of hydrogen adsorption near zero on Pd and Pt nanoislands on Au(111). Electrocatalyst sites with $\Delta G_{H_{ads}} \approx 0$ play an essential role in understanding many aspects of hydrogen oxidation reaction (HOR)/HER on metal electrocatalysts [14–18].

We identify the catalytic sites with $\Delta G_{H_{ads}} \approx 0$ on metal-supported metal nanoislands by simulating the high coverage conditions of adsorbed hydrogen [11] using model Pt and Pd

✉ Juan A. Santana
juan.santana6@upr.edu

Joshua Meléndez-Rivera
joshua.melendez5@upr.edu

[1] Department of Chemistry, University of Puerto Rico at Cayey, Cayey 00737, Puerto Rico

nanoislands of 1–2 nm in diameter. The so-called atomic site catalysts are another class of systems where the preference of hydrogen for low-coordination and high-coordination sites should be clearly understood. Atomic site catalysts are usually single metal atoms or sub-nanosize clusters coordinated with non-metallic or metallic support matrices [19–23]. Atomic site catalysts are typically divided into three main groups: (*i*) single-atom catalyst (SAC), (*ii*) single clusters catalyst (SCC), and (*iii*) single-atom alloy catalyst (SAAC) [20–22, 24, 25]. Each one has the potential for reactions like C–C coupling for the formation of ethane [26], C–C cleavage for ethanol decomposition through steam reforming, formation of CH_4 and CO [27], dehydrogenation [28, 29], and hydrogenation [30]. These catalysts work around common problems such as catalyst and ligands recovery, slow/fast release of adsorbate, selectivity between species, and overall yields.

SAAC, SAC, and SCC of Pt and Pd are among the most studied of these systems [19–23]. Many studies of Pt and Pd catalysts have focused on hydrogen dissociation and binding because of the crucial role of hydrogenation reactions. Tierney et al. performed a combination of experimental and theoretical works to demonstrate the effectiveness in promoting the H_2 dissociation of an inert host metal when alloyed with Pd. On the computational side, calculations have mainly focused on the SAAC of PdAu(111) [31–33] and SCC of Pd/Au [34–39] and Pt/Au [34, 35]. However, there are no systematic computational studies comparing hydrogen adsorption on metal-supported SAAC, SAC, and SCC under high coverage of adsorbed hydrogen. In the present work, we aim to close this gap by exploring high coverage conditions of adsorbed hydrogen on Au-supported atomic site Pt and Pd catalysts.

Methodology

We employed the *Vienna Ab-initio Simulation Package* (VASP) [40–42] for all DFT calculations. The Perdew–Burke–Ernzerhof (PBE) [43] variant of the generalized gradient approximation (GGA) was used to represent exchange–correlation effects. The ionic cores were described by the projector augmented-wave (PAW) [44, 45] method. The electronic one-particle wave functions were expanded on a plane-wave basis to an energy cutoff of 350 eV. The technique of fractional occupation numbers with a level width of 0.05 eV was used. All total energies were extrapolated to $k_bT = 0$ eV. The interaction between the repeated slabs was modified for a dipole correction implemented in VASP. We restricted our calculations to the spin-averaged strategy because adsorption energies of hydrogen evaluated from spin-polarized and spin-averaged calculations differ by only one kJ mol^{-1}.

For the Pd_n/Au(111) and Pt_n/Au(111) ($n = 1$ and 3) systems, calculations were performed with a (4×4) surface model of four atomic layers, separated by a vacuum region over 10 Å. Our model systems are limited to the near-ideal Au(111) surface, where herring-bone reconstruction is not considered, even though they have been experimentally observed [46, 47]. Such reconstructions are outside the focus of the present work. Our computational results are still relevant because, in experimental measurements of Au(111), patches without herring-bone reconstruction are also observed. During geometry optimization, the two "bottom" atomic layers of the surface models were fixed at the calculated lattice constants [48], while the remaining atoms were allowed to relax until all residual forces were less than 0.02 eV/Å. Brillouin zone integrations were carried out with $(5 \times 5 \times 1)$ and $(7 \times 7 \times 1)$ k-point sampling [49] for geometrical optimization and the final results, respectively.

Hydrogen adsorption on Au-supported SAAC, SAC, and SCC was studied by calculating the free energy of adsorption $\Delta G\left(\theta_{H_{ads}}\right)$ as follows:

$$\Delta G\left(\theta_{H_{ads}}\right) \approx \Delta E\left(\theta_{H_{ads}}\right) + 23 \text{ kJ/mol}^{-1} \quad (1)$$

where $\Delta E\left(\theta_{H_{ads}}\right)$ is the differential hydrogen adsorption energy, and 23 kJ mol^{-1} is the difference in zero-point energy and entropy per H_{ads} at 300 K [50, 51]. The differential hydrogen adsorption energy was calculated following Skúlason et al. [52, 53]:

$$\Delta E\left(\theta_{H_{ads}}\right) = \frac{N}{\Delta n}\left[E_{int}(n/N) - E_{int}((n-1)/N)\right] \quad (2)$$

where $E_{int}\left(\theta_{H_{ads}}\right)$ is the integral hydrogen adsorption energy calculated as:

$$E_{int}\left(\theta_{H_{ads}}\right) = \frac{1}{N}\left(E_{tot}(n\text{H@M}) - \frac{n_H}{2}E_{tot}\left(H_2\right) - E_{tot}(\text{M})\right) \quad (3)$$

In Eq. 3, $E_{tot}(n\text{H@M})$, $E_{tot}\left(H_2\right)$, and $E_{tot}(\text{M})$ are the total DFT energy energies of the combined hydrogen/metal system, the hydrogen molecule, and the metal slab, respectively. The number of adsorbed hydrogen atoms is n_H. The number of active surface metal atoms M is N, and $\theta_{H_{ads}} = n_H/N$ is the coverage of adsorbed hydrogen [10, 11, 33, 36]. The calculated bond energy of H_2 is -436 kJ mol^{-1} and -408 kJ mol^{-1} after zero-point energy correction.

Results and Discussion

We studied the effects of adsorbed hydrogen coverage on the adsorption of hydrogen on Au(111)-supported SAC (Pd_1/Au and Pt_1/Au), SAAC (Pd_1Au and Pt_1Au), and SCC (Pd_3/Au and Pt_3/Au). There are multiple atomic configurations for n_H

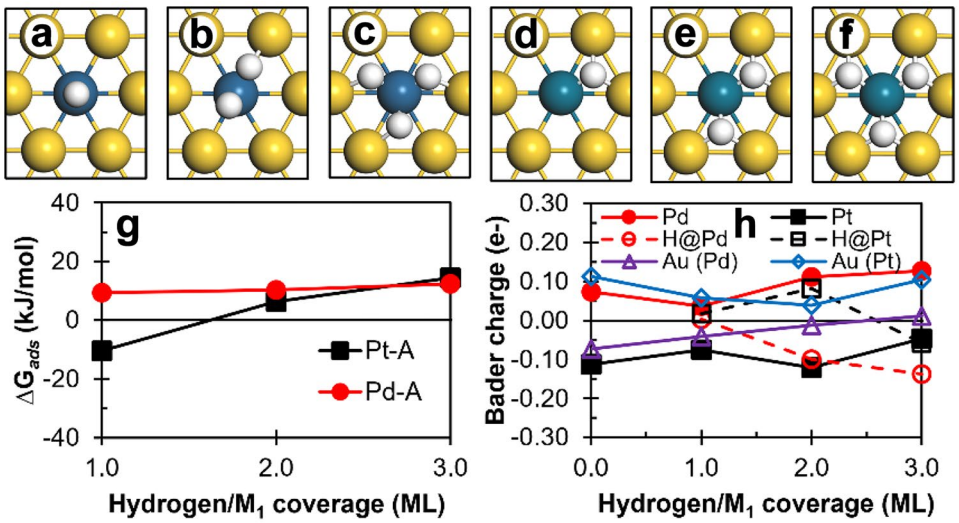

Fig. 1 Properties of adsorbed hydrogen on $Pt_1Au(111)$ and $Pd_1Au(111)$ alloyed surfaces. Panels **a** to **c** show the stable conformations of hydrogen on $Pt_1Au(111)$ and panels **d** to **f** on $Pd_1Au(111)$. Panel **g** displays the free energy of adsorption ΔG_{ads}, and panel **h** shows the average Bader charge on the adsorbed hydrogen atoms, Pt (Pd), and Au(111) atoms. Hydrogen coverage, $\theta_{H_{ads}}$, is defined as the number of hydrogens n_H per active surface metal atoms, M. Numerical values are provided in Table S1 of the Supplementary Information section

hydrogen atoms adsorbed on Pd_n (or Pt_n) on Au(111). We search for low-energy configurations employing standard optimization methods. We also used molecular dynamics (MD) to corroborate the stability of the low-energy atomic structures. In the following, we first discuss our DFT result for adsorbed hydrogen energetic and geometric properties on SAC and SAAC of Pd and Pt. We later discuss the DFT results for hydrogen adsorbed on triangular Pd_3, along with triangular and linear Pt_3 SCC on the Au(111). In discussing the calculated properties of these systems, we focus on three main aspects: (*i*) trend of the free energy of adsorption $\Delta G(\theta_{H_{ads}})$, (*ii*) the oxidation state of adsorbed hydrogen atoms, and (*iii*) finally, the effects of $\theta_{H_{ads}}$ on the spillover of hydrogen from Pd and Pt SAC, SAAC, and SCC onto the Au(111) surface. Please note that we focus on the trend of free energy of adsorption as its numerical values depend on the employed functionals [54]; numerical values are provided in the Supplementary Information (SI) section.

Hydrogen on SAAC and SAC

Figure 1a–c and d–f show the stable conformations of hydrogen on $Pt_1Au(111)$ and $Pd_1Au(111)$ SAAC, respectively. For hydrogen coverage $\theta_{H_{ads}}$ = 1ML, 2ML, 3ML, the adsorption configurations for hydrogen atoms on $Pt_1Au(111)$ correspond to ontop, ontop-bridged, and bridged sites, respectively. For $\theta_{H_{ads}}$ = 1ML, 2ML, 3ML on $Pd_1Au(111)$, the stable hydrogen adsorption sites correspond to threefold configurations (H bonded to the Pd atom and two Au atoms). These configurations were previously reported for $Pt_1Au(111)$ and $Pd_1Au(111)$ [33, 55]. The average nearest-neighbor distances <H–Pd> and <H-Au> are 1.81 and 1.89 Å, respectively, for the various hydrogen coverages. Figure 1g shows the corresponding $\Delta G(\theta_{H_{ads}})$ for the dissociative adsorption of hydrogen. $Pt_1Au(111)$ and $Pd_1Au(111)$ show different $\Delta G(\theta_{H_{ads}})$ profiles. $\Delta G(\theta_{H_{ads}})$ increases with hydrogen coverage in the case of $Pt_1Au(111)$, but stays around 10kJ/mol for $Pd_1Au(111)$ as previously reported [33]. Such difference between $Pt_1Au(111)$ and $Pd_1Au(111)$ comes from hydrogen preferring low coordination on Pt but high coordination of Pd. For $\theta_{H_{ads}}$ = 2ML, 3ML, H_{ads} is partially charge, as shown by the Bader charge analysis in Fig. 1h. The high coordination of hydrogen on $Pd_1Au(111)$ results in longer $H_{ads} - H_{ads}$ separation and less repulsive interaction; see Table S1. In the case of $Pt_1Au(111)$, the preference for lower coordination results in competition between the attractive $Pt - H_{ads}$ and repulsive $H_{ads} - H_{ads}$ interactions. Note that our results of $\Delta G(\theta_{H_{ads}}$ = 1ML) agree very well with the results reported by Darby et al. for $Pt_1Au(111)$ and $Pd_1Au(111)$ [55].

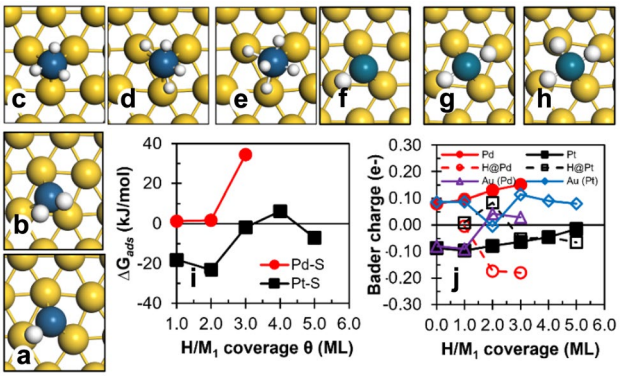

Fig. 2 Properties of adsorbed hydrogen on Pt and Pd atoms supported on Au(111). Panels **a** to **e** show the stable conformations of hydrogen on Pt and panels **f** to **h** on Pd. Panel **i** displays the free energy of adsorption ΔG_{ads}, and panel j shows the total Bader charge on the adsorbed hydrogen atoms, Pt (Pd), and Au(111) atoms. Hydrogen coverage, $\theta_{H_{ads}}$, is defined as the number of hydrogens n_H per active surface metal atoms, M. Numerical values are provided in Table S2 of the Supplementary Information section

Figure 2a–c and d–f show the stable conformation of hydrogen on Pt_1/Au(111) and Pd_1/Au(111) SAC, respectively. For hydrogen coverage $\theta_{H_{ads}} = 1ML, 2ML, 3ML$, the adsorption configurations for hydrogen atoms on Pt_1/Au(111) correspond to distorted ontop, ontop-edge like, and ontop-bridge structures, respectively. For $\theta_{H_{ads}} = 1ML, 2ML, 3ML$, on Pd_1/Au(111), the stable hydrogen adsorption sites correspond to bridge configurations. Figure 2i shows the corresponding $\Delta G(\theta_{H_{ads}})$ for the dissociative adsorption of hydrogen. Contrariry to the SAAC, Pt_1/Au(111) and Pd_1/Au(111) SAC show similar $\Delta G(\theta_{H_{ads}})$ profiles; $\Delta G(\theta_{H_{ads}})$ increase with $\theta_{H_{ads}}$. For Pt_1/Au(111) both $\Delta G(1ML)$ and $\Delta G(2ML)$ are close to $-20kJ/mol$ while for $\theta_{H_{ads}} = 3-5ML$, $\Delta G\left(\theta_{H_{ads}}\right)$ is around $0kJ/mol$. Further saturating of the SAC results in the $\Delta G\left(\theta_{H_{ads}}\right) \ll 0kJ/mol$. In the case of Pd_1/Au(111), $\theta_{H_{ads}} = 1ML, 2ML$ show a $\Delta G\left(\theta_{H_{ads}}\right)$ close to 0 kJ/mol while for $\theta_{H_{ads}} \geq 3ML$, $\Delta G\left(\theta_{H_{ads}}\right) > 0kJ/mol$. For $\theta_{H_{ads}} = 2ML, 3ML$, H_{ads} is partially charge in Pt/Au and Pd/Au as shown by the Bader charge analysis in Fig. 2h.

Hydrogen on SCC

We turn now to the hydrogen adsorption on Pd_3 and Pt_3 clusters on Au(111). Figure 3 shows the low-energy geometrical structures of hydrogen atoms adsorbed on linear Pt_3 and triangular Pt_3 and Pd_3 on Au(111). Other H_{ads} configurations were explored and are included in Fig./Table S3 and S4, of the SI. We include the linear (wired) structure only for Pt_3 since wired Pd_3 is not the preferred structure on Au(111). The stability of wired Pt_3 on Au(111) was first pointed out in the work of Schulte et al. [34]. We recently showed that the relative stability of this linear structure might come from steric repulsion in the triangular conformation of Pt_3 because linear structures are not the preferred conformations for larger Pt clusters on Au(111) [54].

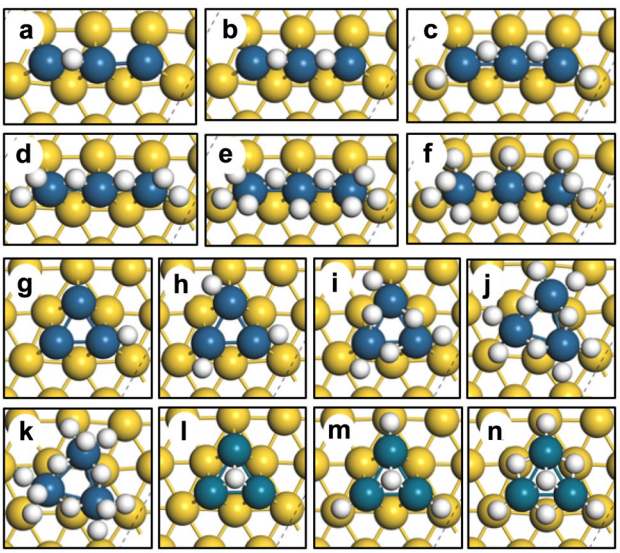

Fig. 3 Panels **a** to **f** show stable conformations of 1 to 12 hydrogen atoms adsorbed on a Pt_3 linear cluster (Pt_3-L). Panels **g** to **k** correspond to the stable conformations of 1 to 12 hydrogen atoms on a Pt_3 triangular cluster (Pt_3-T). Panels **l** to **n** show stable conformations of 1 to 7 hydrogen atoms on a Pd_3 triangular cluster

For the linear Pt cluster (Pt_3-L), hydrogen with $\theta_{H_{ads}} \leq 4/3ML$ is located on bridge sites. For $\theta_{H_{ads}} = 2ML$, hydrogen atoms are on-top position with an average-nearest neighbor distance of 2.7 Å between H atoms; see Table S4. For triangular-arranged systems, the adsorption configurations for hydrogen atoms are different on Pd_3 and Pt_3 for $\theta_{H_{ads}} \leq 1ML$. On Pd_3, one hydrogen is located on the hollow site, and the other hydrogen atoms are at the Pd_3/Au boundary (the rim sites), where hydrogen is coordinated to both Pd and Au. In the case of Pt_3, all hydrogen atoms are at Pt/Au boundary, where hydrogen atoms are single-coordinated to Pt, lying parallel to the Au(111) surface with Au-H distances over 2.7 Å. These results at low coverage of adsorbed hydrogen agree with previous calculations on Pd [34–39] and Pt [34, 35] nanoislands on Au(111). At hydrogen coverage $\theta_{H_{ads}} \geq 5/3ML$, the adsorption configurations are also different for Pd_3 and Pt_3; the hydrogen atoms are on the hollow, rim, and bridge sites on Pd_3 and on bridge, rim and on-top sites on Pt_3.

Figure 4 a shows $\Delta G\left(\theta_{H_{ads}}\right)$ for the dissociative adsorption of hydrogen on Pd_3 and Pt_3 on Au(111). At very low $\theta_{H_{ads}}$, ΔG is below $-30kJ/mol$ for all SCC systems. Increasing hydrogen coverage starts showing different $\Delta G\left(\theta_{H_{ads}}\right)$ behavior between Pd_3 and Pt_3. For $\theta_{H_{ads}} = 2/3-4/3ML$ in Pd_3, $\Delta G\left(\theta_{H_{ads}}\right) \approx 0kJ/mol$ suggesting that the active sites will be at the Pd/Au boundary. For $\theta_{H_{ads}} \geq 5/3ML$, $\Delta G\left(\theta_{H_{ads}}\right) > 0$ suggesting that no other sites are active on Pd_3/Au. Such findings align with the work of Liang et al. [9], showing that the catalytic activity for HER is maximal at the Pd/Au boundary in Pd nanoislands on Au(111). For linear and triangular Pt_3 clusters, the situation is different, and there are multiple sites with $\Delta G\left(\theta_{H_{ads}}\right) \approx 0$. At hydrogen coverages of $\theta_{H_{ads}}$ of 6/3ML, 9/3ML, and 12/3ML on Pt_3/Au, adsorption on the bridge, ontop, and Pt/Au boundary sites have $\Delta G\left(\theta_{H_{ads}}\right) \approx 0$. These results indicate that there could be various active sites for Pt_3/Au as we recently reported [11] for nanoislands of Pt/Au.

Figure 4b and c shows the Bader charge for hydrogen, Pt (Pd), and Au atoms in the systems comprised of Pt_3-L and triangular Pt_3 and Pd_3 supported on Au(111). The Bader charge analysis indicates that the charge transfer processes differ on Pd_3/Au and Pt_3/Au, but they can also vary through geometrical configurations. On triangular Pd_3/Au, the charge is transferred from both Pd and Au to the hydrogen atoms. In triangular and linear Pt_3/Au, the charge is mainly transferred from the Au surface to the hydrogen atoms.

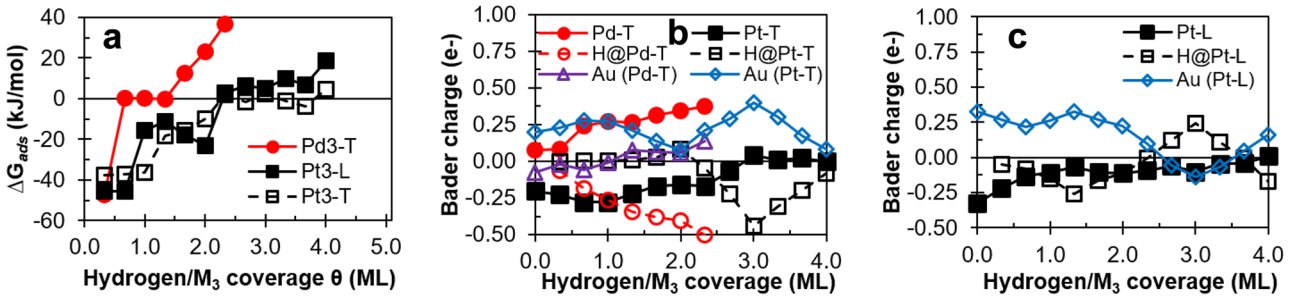

Fig. 4 **a** Free energy of adsorption ΔG_{ads} as function of hydrogen coverage on Pt_3 and Pd_3 on Au(111). Panels **b** and **c** show the total Bader charge of Pd_3, Pt_3, adsorbed H atoms, and Au(111) atoms. Note that for Pt_3, results are shown for clusters with linear (Pt-L) and triangular (Pt-T) conformations. Hydrogen coverage, $\theta_{H_{ads}}$, is defined as the number of hydrogens n_H per active surface metal atoms, M. Numerical values are provided in Table S3 and S4 of the Supplementary Information section.

Hydrogen Spillover from SAAC, SAC, and SCC

The effects of $\theta_{H_{ads}}$ on the spillover of hydrogen from Pd (or Pt) to the Au(111) surface was studied by calculating the diffusion energy E_{diff}; the energy change due to hydrogen migration from the Pd (or Pt) metal to the Au(111) surface [31, 35]. E_{diff} is the so-called thermodynamic barrier. The kinetic barrier or activation energy (E_{act}) is expected to be 10–15 kJ/mol higher that E_{diff}, based on our previous calculations for hydrogen spillover on Pd_3 and Pt_3 on Au(111) under low coverage conditions of adsorbed hydrogen [35]. The hollow site on the Au-substrate directly accessible from diffusion was chosen as the final location. The E_{diff} for SAAC and SAC of Pt and Pd are included in Table S5 and S6 of the Supporting Information sections. In both SAAC and SAC, E_{diff} is generally over 20 kJ/mol. Note that the spillover of hydrogen atoms from Pd-SAAC to Au sites can be enhanced by coadsorption of CO [32].

Figure 5 shows E_{diff} as a function of the hydrogen coverage $\theta_{H_{ads}}$ for Pt_3/Au and Pd_3/Au. For every hydrogen coverage studied for Pt_3/Au and Pd_3/Au, the least stable adsorbed hydrogen atom was simulated to migrate from Pt (or Pd) to Au(111). In the case of Pt_3/Au, such a direct diffusion pathway is unlikely, but it provided a lower-bound estimate of the diffusion energy. Up to $\theta_{H_{ads}} = 1$ML, E_{diff} is close to 40 kJ mol^{-1} and 80 on Pd_3 and Pt_3, respectively. At hydrogen coverage of $\theta_{H_{ads}} \geq 2$ML, the diffusion energy is reduced to $\sim 20 kJ/mol^{-1}$ in the case of Pd_3. In the case of Pt_3, the lowest value of E_{diff} is around 40 kJ mol^{-1}. These calculated energies show that hydrogen spillover from supported Pd_3 or Pt_3 to well-defined Au(111) is not thermodynamically favorable [31] even under high hydrogen coverage conditions. This result reflects the low reactivity of well-defined Au surfaces toward the hydrogen dissociate adsorption, $\Delta G \approx 30 kJ/mol$ for hydrogen adsortion on Au(111). However, hydrogen diffusion could be thermodynamically feasible from SCC to an Au surface with adatoms, surface alloys,

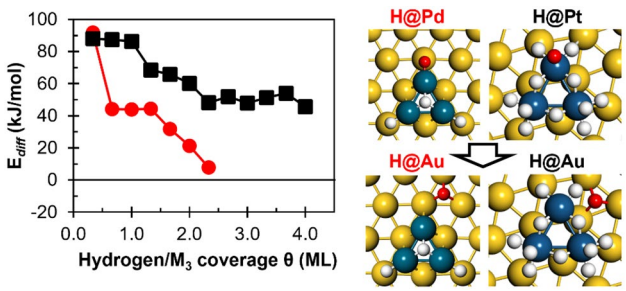

Fig. 5 Hydrogen diffusion energy as a function of the initial hydrogen coverage on Au-supported Pt_3 and Pd_3. The hydrogen undergoing diffusion is highlighted in red in the righthand panels. The horizontal line indicates $E_{diff} = 0$. Hydrogen coverage, $\theta_{H_{ads}}$, is defined as the number of hydrogens n_H per active surface metal atoms, M. Numerical values are provided in Tables S5–S7 of the Supplementary Information section

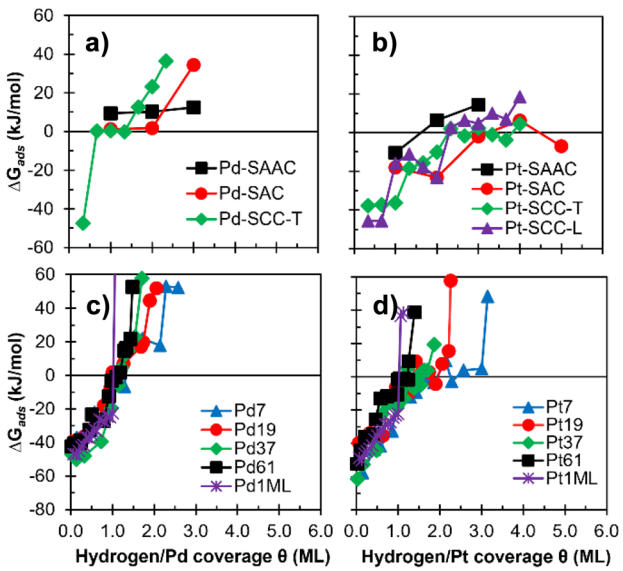

Fig. 6 Comparison of free energy of adsorption ΔG_{ads} as function of hydrogen coverage on Au-supported Pt and Pd SAAC, SAC, SCC, nanoislands, and overlayered systems. Hydrogen coverage, $\theta_{H_{ads}}$, is defined as the number of hydrogens n_H per active surface metal atoms M

or other defects, as a comparison of $\Delta G(\theta_{H_{ads}})$ for SAAC, SAC, and SCC suggests.

Comparison of Hydrogen Adsorption On SAAC, SAC, SCC, Nanoislands, and Overlayered Surfaces

We now compare our results for the hydrogen adsorption on SAAC, SAC, and SCC. Figure 6 shows the free energy of adsorption $\Delta G(\theta_{H_{ads}})$ as function of hydrogen coverage on SAAC, SAC, and SCC of Pd/Au and Pt/Au systems. For further comparison, we also include Fig. 6 $\Delta G(\theta_{H_{ads}})$ for nanoislands and overlayers of Pd/Au and Pt/Au reported in our previous work [11]. Pd/Au and Pt/Au have different $\Delta G(\theta_{H_{ads}})$ profiles for SAAC, SAC, SCC, and small nanoislands (nuclearity < 37). In general, $\Delta G(\theta_{H_{ads}})$ is centered around 0kJ/mol for hydrogen coverages near 1 ML on the SAAC, SAC, and SCC of Pd/Au. $\Delta G(\theta_{H_{ads}})$ is below −10kJ/mol for 1 ML of hydrogen on the corresponding Pt/Au systems. The maximum hydrogen coverage is another clear difference between Pt/Au and Pd/Au systems. The maximum hydrogen coverage is the coverage of adsorbed hydrogen where $\Delta G(\theta_{H_{ads}}) \approx 0$, and it plays an important role in understanding many aspects of HOR/HER on metal catalysts [14, 15]. The maximum hydrogen coverage is also crucial to help identify the nature of the active site for HOR/HER [16–18]. Generally, the maximum hydrogen coverage for SAAC, SAC, SCC, and small nanoislands (nuclearity < 37) in Pt/Au is twice or more than in Pd/Au. Such effect fades away as the ratio of edge to terrace sites diminishes, and the maximum hydrogen coverage is similar for large nanoislands and overlayered Pt/Au and Pd/Au. The preference of hydrogen for low-coordination results in higher hydrogen coverage on edge-rich Pt/Au systems.

Conclusions

DFT calculations were performed to study the adsorption of hydrogen under high coverage conditions of adsorbed hydrogen on single atom alloy catalyst (SAAC), single-atom catalyst (SAC), and single clusters catalyst (SCC) of Pd and Pt on Au(111). The computational results show that under high coverage conditions of adsorbed hydrogen, there are more adsorption sites for hydrogen on Pt/Au than on Pd/Au systems. The preference of hydrogen for low coordination on Pt results in a higher number of adsorption sites on Pt/Au systems. Moreover, the adsorption sites on Pt/Au have a free energy of hydrogen adsorption near zero, which can help understand the different catalytic properties of Pd/Au and Pt/Au for hydrogen reactions.

Supplementary Information The online version contains supplementary material available at https://doi.org/10.1007/s12678-022-00802-x.

Author Contribution J.M.R.: data curation, formal analysis, methodology, investigation, visualization, writing—original draft, writing review and editing. J.A.S.: conceptualization, formal analysis, funding acquisition, project administration, supervision, visualization, writing—review and editing.

Funding This work was supported by the startup funding provided by the Offices of the Chancellor and the Dean of Academic Affairs of the University of Puerto Rico at Cayey. J.M.R. was supported by the "Fondo Institucional para el Desarrollo de la Investigación (FIDI 2019–2020)" of the University of Puerto Rico at Cayey and the National Aeronautics and Space Administration (NASA) Training Grant No. NNX15AI11H. Calculations were performed on the computing facility at the University of Puerto Rico at Cayey, which is supported in part by the National Institute of General Medical Sciences of the National Institutes of Health through Grant NIH NIGMS/INBRE P20GM103475-15. Its contents are solely the responsibility of the authors and do not necessarily represent the official view of the NIGMS or NIH. J.A.S.: National Institute of General Medical Sciences of the National Institutes of Health through Grant NIH NIGMS/INBRE P20GM103475-15; The National Aeronautics and Space Administration (NASA) Training Grant No. NNX15AI11H.

Availability of Data and Material Not applicable.

Declarations

Ethics Approval Not applicable.

Consent to Participate Not applicable.

Consent for Publication Not applicable.

Conflicts of Interest The authors declare no competing interests.

References

1. D. Huang, N. He, Q. Zhu, C. Chu, S. Weon, K. Rigby, X. Zhou, L. Xu, J. Niu, E. Stavitski, J.-H. Kim, ACS Catal. **11**, 5586 (2021)
2. T. Ricciardulli, S. Gorthy, J.S. Adams, C. Thompson, A.M. Karim, M. Neurock, D.W. Flaherty, J. Am. Chem. Soc. (2021)
3. J.A. Trindell, Z. Duan, G. Henkelman, R.M. Crooks, Chem. Rev. **120**, 814 (2020)
4. C. Xie, Z. Niu, D. Kim, M. Li, P. Yang, Chem. Rev. **120**, 1184 (2020)
5. J. Berwanger, S. Polesya, S. Mankovsky, H. Ebert, F.J. Giessibl, Phys. Rev. Lett. **124**, 096001 (2020)
6. S. Hou, R.M. Kluge, R.W. Haid, E.L. Gubanova, S.A. Watzele, A.S. Bandarenka, B. Garlyyev, ChemElectroChem **8**, 3433 (2021)
7. M. Lunardon, T. Kosmala, C. Dr, S. Agnoli, G. Granozzi, Joule **6**, 617 (2022)
8. J.H.K. Pfisterer, Y. Liang, O. Schneider, A.S. Bandarenka, Nature **549**, 74 (2017)
9. Y. Liang, C. Csoklich, D. McLaughlin, O. Schneider, A.S. Bandarenka, A.C.S. Appl, Mater. Interfaces **11**, 12476 (2019)
10. J.A. Santana, B. Cruz, J. Melendez-Rivera, N. Rösch, J. Phys. Chem. C **124**, 13225 (2020)
11. J.A. Santana, J. Meléndez-Rivera, J. Phys. Chem. C **125**, 5110 (2021)
12. G. Seifert, H.-G. Fritsche, P. Ziesche, V. Heera, Phys. Status Solidi B **121**, 705 (1984)
13. K. Balasubramanian, P.Y. Feng, M.Z. Liao, J. Chem. Phys. **87**, 3981 (1987)

14. E. Santos, P. Hindelang, P. Quaino, E.N. Schulz, G. Soldano, W. Schmickler, ChemPhysChem **12**, 2274 (2011)
15. F. Yang, Q. Zhang, Y. Liu, S. Chen, J. Phys. Chem. C **115**, 19311 (2011)
16. P. Lindgren, G. Kastlunger, A.A. Peterson, ACS Catal. **10**, 121 (2020)
17. M.T. Tang, X. Liu, Y. Ji, J.K. Norskov, K. Chan, J. Phys. Chem. C **124**, 28083 (2020)
18. K.S. Exner, Angew. Chem. Int. Ed. **59**, 10236 (2020)
19. F. Zaera, Chem. Rev. **122**, 8594 (2022)
20. S. Mitchell, J. Pérez-Ramírez, Nat. Commun. **11**, 4302 (2020)
21. E.C.H. Sykes, P. Christopher, Curr. Opin. Chem. Eng. **29**, 67 (2020)
22. J. Mao, J. Yin, J. Pei, D. Wang, Y. Li, Nano Today **34**, 100917 (2020)
23. Z.-K. Han, D. Sarker, R. Ouyang, A. Mazheika, Y. Gao, S.V. Levchenko, Nat. Commun. **12**, 1833 (2021)
24. B.C. Gates, Trends Chem. **1**, 99 (2019)
25. F. Maroun, F. Ozanam, O.M. Magnussen, R.J. Behm, Science **293**, 1811 (2001)
26. R. Réocreux, M. Uhlman, T. Thuening, P. Kress, R. Hannagan, M. Stamatakis, E.C.H. Sykes, Chem. Commun. **55**, 15085 (2019)
27. H. Li, E.J. Evans, C.B. Mullins, G. Henkelman, J. Phys. Chem. C **122**, 22024 (2018)
28. T. Duan, R. Zhang, L. Ling, B. Wang, J. Phys. Chem. C **120**, 2234 (2016)
29. Z. Li, T. He, D. Matsumura, S. Miao, A. Wu, L. Liu, G. Wu, P. Chen, ACS Catal. **7**, 6762 (2017)
30. K. Yang, B. Yang, J. Phys. Chem. C **122**, 10883 (2018)
31. H.L. Tierney, A.E. Baber, J.R. Kitchin, E.C.H. Sykes, Phys. Rev. Lett. **103**, (2009)
32. F.R. Lucci, M.T. Darby, M.F.G. Mattera, C.J. Ivimey, A.J. Therrien, A. Michaelides, M. Stamatakis, E.C.H. Sykes, J. Phys. Chem. Lett. **7**, 480 (2016)
33. S. Venkatachalam, T. Jacob, Phys. Chem. Chem. Phys. **11**, 3263 (2009)
34. E. Schulte, E. Santos, P. Quaino, Surf. Sci. 121605 (2020)
35. J.A. Santana, N. Rösch, Phys. Chem. Chem. Phys. **14**, 16062 (2012)
36. P. Quaino, E. Santos, H. Wolfschmidt, M.A. Montero, U. Stimming, Catal. Today **177**, 55 (2011)
37. M.E. Björketun, G.S. Karlberg, J. Rossmeisl, I. Chorkendorff, H. Wolfschmidt, U. Stimming, J.K. Nørskov, Phys. Rev. B **84**, 045407 (2011)
38. A. Roudgar, A. Groß, Surf. Sci. **559**, L180 (2004)
39. J. Andersin, K. Honkala, Phys. Chem. Chem. Phys. **13**, 1386 (2011)
40. G. Kresse, J. Hafner, Phys. Rev. B **47**, 558 (1993)
41. G. Kresse, J. Hafner, Phys. Rev. B **49**, 14251 (1994)
42. G. Kresse, J. Furthmüller, Phys. Rev. B **54**, 11169 (1996)
43. J.P. Perdew, K. Burke, M. Ernzerhof, Phys. Rev. Lett. **77**, 3865 (1996)
44. P.E. Blöchl, Phys. Rev. B **50**, 17953 (1994)
45. G. Kresse, D. Joubert, Phys. Rev. B **59**, 1758 (1999)
46. S. Narasimhan, D. Vanderbilt, Phys. Rev. Lett. **69**, 1564 (1992)
47. H. Walen, D.-J. Liu, J. Oh, H. Lim, J.W. Evans, Y. Kim, P.A. Thiel, J. Chem. Phys. **143**, 014704 (2015)
48. J.A. Santana, N. Rösch, J. Phys. Chem. C **116**, 10057 (2012)
49. H.J. Monkhorst, J.D. Pack, Phys. Rev. B **13**, 5188 (1976)
50. J.K. Nørskov, T. Bligaard, A. Logadottir, J.R. Kitchin, J.G. Chen, S. Pandelov, U. Stimming, J. Electrochem. Soc. **152**, J23 (2005)
51. J. Greeley, J.K. Nørskov, L.A. Kibler, A.M. El-Aziz, D.M. Kolb, ChemPhysChem **7**, 1032 (2006)
52. E. Skúlason, G.S. Karlberg, J. Rossmeisl, T. Bligaard, J. Greeley, H. Jónsson, J.K. Nørskov, Phys. Chem. Chem. Phys. **9**, 3241 (2007)
53. E. Skúlason, V. Tripkovic, M.E. Björketun, S. Gudmundsdóttir, G. Karlberg, J. Rossmeisl, T. Bligaard, H. Jónsson, J.K. Nørskov, J. Phys. Chem. C **114**, 18182 (2010)
54. G.A. Vázquez-Lizardi, L.A. Ruiz-Casanova, R.M. Cruz-Sánchez, J.A. Santana, Surf. Sci. **712**, 121889 (2021)
55. M.T. Darby, R. Réocreux, E. Charles. H. Sykes, A. Michaelides, M. Stamatakis, ACS Catal. **8**, 5038 (2018)